IEEE Access
Multidisciplinary | Rapid Review | Open Access Journal

Received April 24, 2021, accepted May 10, 2021, date of publication May 21, 2021, date of current version June 2, 2021.

Digital Object Identifier 10.1109/ACCESS.2021.3082846

An Improved Decomposition as a Trade-Off Between Utilizing Unitary Matrix Rotations and New Scattering Models

AMIT KUMAR[1], (Student Member, IEEE), HIMANSHU MAURYA[2], ARUNDHATI RAY MISRA[3], AND RAJIB KUMAR PANIGRAHI[1], (Senior Member, IEEE)

[1]Department of Electronics and Communication Engineering, IIT Roorkee, Roorkee 247667, India
[2]Department of Electronics and Communication Engineering, Indian Institute of Information Technology Allahabad, Prayagraj 211015, India
[3]Space Applications Centre, Indian Space Research Organisation, Ahmedabad 380015, India

Corresponding author: Rajib Kumar Panigrahi (rajibpanigrahi@ieee.org)

This work was supported by the Space Applications Centre, Indian Space Research Organization, Ahmadabad, India, through the Airborne L&S SAR Project AO, under Grant EPSA/3.1.1/2017.

ABSTRACT The requirement of an efficient decomposition technique has always been a priority in the field of physical model-based scattering power decomposition. In view of this, the presented work has been carried out in two sections. In the first part, two parallel model-based approaches have critically been analyzed based on their decomposition strategy, result, and limitations. Considering the challenges, the second section emerges out with an improved seven-component (7*SR*) decomposition technique. The proposed architecture is ideally based on embedding the best attributes of both the parallel approaches under one roof. The productivity of the introduced method has been validated on ALOS PALSAR-2 datasets over the San Francisco Bay Area, CA, USA, and Mumbai, India. Algorithmic simplicity and proper distribution of decomposed scattering powers are maintained as the results have been obtained without considering any power restriction constraints. The work shows an enhancement in the underlined dominant scattering mechanism. Simultaneously, a tremendous suppression in the percentage of negative scattering pixels is also achieved, making the 7*SR* algorithm special among its class.

INDEX TERMS Model-based decomposition, negative scattering pixels, SAR polarimetry, unitary rotations, seven-component decomposition.

I. INTRODUCTION

Enhancement towards anthropogenic forcing occurring across the world demanded the requirement of some specific technique through which the developments can efficiently be monitored. To execute this, one of the best promising approaches is microwave remote sensing incorporating polarimetric synthetic aperture radar (polSAR) techniques. The information extraction from polSAR datasets has played a significant role in analyzing land covers related to earth and other celestial bodies. A pixel in polSAR image represents a particular terrain, interpreted by a unique covariance ($[C]$) or coherency ($[T]$) matrix. The retrieval of information from the coherency matrix is generally carried out through target decomposition techniques. Among available approaches, the model-based strategy has cemented its position based on its superior performance in terrain characterization, algorithmic simplicity, and ease of implementation. The first model-based decomposition was introduced by Freeman and Durden in their three-component scattering (*TCD*) model [1]. In this technique, the measured coherency matrix was decomposed as a linear summation of three primary scattering mechanisms, viz. single or odd bounce scattering from a moderately rough surface, double or even bounce scattering from two orthogonal dielectric surfaces, and volume scattering from a cloud of oriented dipoles. Following the *TCD*, to enhance the decomposition results, the main focus has been given on the complete utilization of the elements of the coherency matrix. Complete utilization leads to retrieval of maximum information that in turn leads to a better target decomposition. Exploration of techniques reported in the literature to achieve this objective has been ended up resulting

The associate editor coordinating the review of this manuscript and approving it for publication was Fan Zhang.

in two parallel approaches: the addition of new scattering models and the incorporation of unitary matrix rotations

A. EVOLUTION OF SCATTERING MODELS

Progression towards the new scattering model had ideally been centered on limitations associated with the Freeman's *TCD* model. As it was based on the assumption of reflection symmetry condition, the cross-correlation terms were assumed to zero ($T_{13} = T_{23} = 0$). Absentia of proper modeling of these elements resulted in the non-utilization of complete polarimetry information. Here, only five out of nine elements have been utilized to show the scattering properties through three components. Yamaguchi *et al.* [2] focused on the aforementioned problem and added helix scattering as the fourth component to address $\Im(T_{23})$ element of the coherency matrix. The helix component was assumed to be present in complex man-made structures. This four-component ($Y4O$) approach was first step towards defining the secondary scattering mechanism, which successfully accounted for six out of nine coherency matrix elements. Furthermore, considering the feature of total randomness, a new volume scattering model was proposed by An *et al.* [3] in the form of an identity matrix. However, in order to fit different forest structures, it was necessary to provide more flexibility in modeling. Hence, several remarkable contributions had been proposed in the area [4]–[9]. For the dihedral subcategory, a few of the significant models have also been introduced [10]–[12].

To provide better segregation of *HV* scattering coming from the complex man-made structures, Xiang *et al.* [13], [14] modified the Yamaguchi's *FCD* by introducing a cross-scattering model using the rotated dihedral corner reflectors and building orientation angle. Additionally, by addressing the cross-scattering model and the eigenvalues of [T], a new scattering model has been proposed by Quan et. al. [15] dedicated to analyzing the scattering contributions from the obliquely oriented building blocks more efficiently. In a series of advancements, Maurya *et al.* [16] proposed an extended four-component decomposition by incorporating a rotated dihedral corner reflector to model the oriented dihedral structures utilizing seven out of nine elements. The further improvement introduced a few more components, usually prevalent in the complex terrain corresponding to cross-correlation elements. Through six-component scattering decomposition ($6SD$) model by Singh and Yamaguchi [17], scattering contributions from oriented and compounded dipoles have been introduced in the form of two additional physical scattering sub-models for $\Re/\Im(T_{13})$. The approach utilized eight out of nine elements. The long-awaited requirement of assigning a proper physical meaning to each coherency matrix element has finally been fulfilled by introducing scattering from the mixed dipoles in the seven-component decomposition ($7SD$) model [18]. Hence, the way out for accounting the unused cross-correlation elements and implementing them into the decomposition for the complete utilization of the polarimetry information has successfully been accomplished.

Nevertheless, defining the secondary scattering mechanism enhances the classification accuracy, but somewhere makes the model-based decomposition technique a bit complex. Simultaneously, it is also observed that with the increase in a number of components, the negative scattering pixels have also been increased drastically. These pixels can forcefully be neutralized by incorporating power restriction constraints. However doing so, it wrecks the power distribution within the span and compromises the accuracy of the decomposition.

B. INCORPORATION OF UNITARY MATRIX ROTATIONS

The concept of orientation angle in the form of desying operation was firstly introduced by Huynen [19], [20] and was further extended by Xu and Jin [21], where the terminology deorientation was introduced to deal with the minimization of cross-polarization HV component. Furthermore, the idea has been incorporated into model-based decomposition as the orientation angle compensation (OAC) by An *et al.* [3] for *TCD*. It comes into picture where complex terrain often gets misclassified as a result of coupling between the orthogonal states of polarization. This usually happens when the cross-polarization component gets generated in the dominant surface and dihedral prone areas. To neutralize such couplings, the coherency matrix is rotated by an angle about the line of sight of the radar. The motive behind deorientation is to minimize the power of the cross-polarization term by utilizing the idea of matrix rotation theory. For complete utilization of coherency matrix elements, unitary matrix rotation theory was introduced and served in two ways. First was to remove the unused elements in order to strengthen the dominant scattering mechanism [3], [22], [24], [26] and the second method was based on the rotation of scattering models [11], [27], [29], [36].

The first approach dealt with the inclusion of unitary rotations on the elements of the coherency matrix. Here, the minimized cross-polarization power from the T_{33} channel contributed towards the magnification of underlined dominant co-polar scattering channels. In view of this, Yamaguchi *et al.* [22] applied OAC before carrying out decomposition for the targets. While in a detailed manner, Lee and Ainsworth [23] has demonstrated the effect of OAC on each element of the coherency matrix. To make the decomposition more efficient, general four-component decomposition ($G4U$) was proposed by Singh *et al.* [24], ideally being concentrated on helix angle compensation. The model was first of its type, where the concept of double unitary rotations has been incorporated. Moreover, Bhattacharya *et al.* [25] presented an adaptive unitary rotation of the coherency matrix ($AG4U$) based on the degree of polarization. Series of exploration led Maurya and Panigrahi [26] to incorporate a pair of special unitary matrices from $SU(3)$ group to eliminate T_{13} completely. Undoubtedly, the exclusion of cross-correlation elements reduces the complexity of decomposition. However, an adverse effect on the decomposition is also observed. As these elements contain

some vital polarimetry information, their elimination limits the target characterization capability of the model-based technique. Moreover, the classification accuracy is hampered as the strategy do not always provide the assurance that the surface and dihedral components would be rotated back to zero cross-polarization power.

Accounting the fact, the second approach in unitary matrix rotation theory was based on the generalization of even and odd bounce scattering models with their orientation angles to fit the off-diagonal terms along with the cross-polarization component. In this regard, Chen *et al.* [27] generalized both the surface and dihedral model by separating their orientation angles in order to account for the cross-polarization power. Aforementioned architecture makes the complete utilization of the polarimetric information. Exploiting both the rotation approaches, noteworthy improvements have been reported regarding the suppression of negative scattering pixels. Nevertheless, accounting for the seven components along with the incorporation of rotation theory is still an issue that needs to be tackled.

C. CHALLENGES IN ACHIEVING THE COMPLETE UTILIZATION

From the uniform *TCD* model [1], as $P_v = 4T_{33}$, volume scattering contribution can solely be determined by the cross-polarization component. The strategy mentioned above is considered the main weakness of *TCD* as it will result in a high volume scattering power, leading to an overestimation in P_v. Simultaneously, the approach might make P_s and P_d negative for some pixels [23]. Yajima *et al.* [28] went through the technical deficiencies of *TCD* and proposed power restriction constraints that force the decomposed results to be non-negative. Meanwhile, hybrid scattering models introduced by Cloude [29] also succeeded in reducing such negative pixels. Van Zyl *et al.* [30] modified the Freeman's *TCD* model by using constraints and proposed a non-negative eigenvalue decomposition method. Cui *et al.* [31] incorporated eigen-decomposition and model fitting approach to tackle the ambiguities related to the complete utilization and negative pixels. However, soon after the incorporation of *OAC* [3], [23], it was concluded that the negative power issue can be minimized, as it dealt with the reduction of cross-polarization power from the dominant scattering mechanism. Furthermore, Cloude's hybrid model [29] has significantly been improved by the incorporation of *OAC* by Singh *et al.* [32]. In recent developments, the chaotic nature of volume scattering phenomena has been addressed by the inclusion of sub-scattering models. However, the negative scattering pixels has also been found to increase.

It is well known that if the scattering power of any component is overestimated, it is compensated by the underestimation of power in other components. Hence, to reduce the overestimation of P_v, in 7*SD*, scattering power analogous to helix, mixed, oriented, and compounded dipole have been subtracted from the T_{33}. However, excluding the contributions of these new scattering components result in underestimation of P_v. Since, P_v is determined through T_{33}, it ultimately becomes negative for some pixels. In addition, the surface and dihedral scattering powers occasionally become negative for some pixels. It is a known fact that the Radar Cross Section (*RCS*) being proportional to the back-scattered power received by the polarimetric radar system can never be negative or zero. In model-based techniques, the back-scattered power is distributed among the scattering components. If the model is accurate, then the power distribution in all components will be non-zero and non-negative. Nevertheless, if a model estimates negative power for any of the scattering components, then it indicates that the model is inaccurate and invalid. Many recent model-based techniques follow the notion that if the scattering power contribution of any component is negative, then it is made zero either forcefully or logically. However, logically, it cannot be zero as it must have some finite positive value. The modified algorithm incorporating power constraints somehow manages to achieve the decomposition with less or zero negative scattering pixels. Nevertheless, this makes the approach more complicated by disorganizing the distribution of power, as the scattering contributions depend on span which remains preserved. Mathematically, an elimination of scattering contribution of any fundamental scattering component skews the power distribution and challenges the algorithmic simplicity. As a result, efficient decomposition and distribution of scattering power cannot be achieved. Recently, the problem of negative scattering pixels has been resolved in three- and four-component [33]–[35], but for the seven-component decomposition, it remains an open problem.

The applicability of each approach, whether the new scattering models or unitary matrix rotations, introduced to enhance the decomposition, should be evaluated on the basis of challenges encountered by the model-based decomposition techniques. The presented work in this paper briefly reviews the technical deficiencies associated with the advancements made in both the methods. Overall, a rigorous comparison of the two parallel approaches has been carried out and reported. While analyzing the results, it is found that both decomposition strategies comprise noteworthy features making them unique among their class. As a trade-off, an improved seven-component decomposition model has been developed. Attempts have been made so that the best attributes of both the schemes can be embedded into a single algorithm. The added advantage is that the results have been obtained without considering any power restriction constraints. Hence, the accuracy of decomposition has been maintained with the proper distribution of decomposed scattering power. To check its applicability against the parallel 7*SD* method, 7*SR* has been implemented on datasets belonging to two different areas. Quantitative analysis of the result shows that 7*SR* proved its productivity in magnifying the power associated with the dominant scattering mechanism. Furthermore, accounting 7*SD*, the result shows that the proposed approach is capable of reducing the negative scattering pixels count to a significantly large amount while maintaining the classification accuracy.

The remaining sections of the paper are organized as follows: An improved seven-component decomposition method has been proposed and briefly been explained in Section II. Here, basic formulations associated with the new scattering models and unitary matrix rotations theory have been explained. Additionally, algorithm of the introduced approach has also been elaborated. The compatibility of 7*SR* with the ALOS PALSAR 2 datasets of Bay area and Mumbai has been discussed in Section III, whereas Section IV concludes the paper.

II. AN IMPROVED APPROACH AS A TRADE-OFF

Accounting challenges, an improved decomposition method has been proposed, considered being a trade-off, where the best attributes of unitary matrix rotations theory and new scattering models have been exploited within a single decomposition scheme. In an attempt to preserve the distribution of power and maintain algorithmic simplicity, the approach has been carried out without considering any power restriction constraints. Moreover, the dominant scattering mechanism has been defined considering an appropriate branching condition that follows the rotations of the coherency matrix elements prior to decomposition. Two special unitary matrix has been incorporated. Each consisting a pair of real and complex rotation matrix to neutralize the coupling between the components $\Re/\Im(T_{13})$ and $\Re/\Im(T_{23})$. The proposed approach reduces the contribution of T_{33} from odd and even-bounce terrains and provides additional information by redistributing the minimized power from the cross-polarization channel back to the underlined dominant co-polarization scattering channels. Maintaining the contributions from the primary three mechanisms, a cross-correlation component gets neutralized at each dominant scattering scenario, and decomposition is being performed through the remaining five components. The complete flow of the work has been demonstrated through the flowchart mention in Figure 1.

Measured coherency matrix (1) as shown at the bottom of the page, can be seen as the polarimetric contribution from nine independent elements. The development of sub-matrices can express the physical scattering mechanism belonging to its seven elements as [18]

$$[T] = f_s[T]_s + f_d[T]_d + \frac{f_v}{4}[T]_v^{uniform} + \frac{f_c}{2}[T]_c + \frac{f_{od}}{2}[T]_{od} + \frac{f_{cd}}{2}[T]_{cd} + \frac{f_{md}}{2}[T]_{md} \quad (2)$$

where, $[T]_s$, $[T]_d$, $[T]_v$, $[T]_c$, $[T]_{od}$, $[T]_{cd}$ and $[T]_{md}$ are the coherency matrix related to the odd-bounce, even-bounce, volume (uniform distribution), helix, oriented, compounded and mixed-dipole scatterings, respectively. Whereas, f_s, f_d, f_v, f_c, f_{od}, f_{cd} and f_{md} are corresponding unknown expansion co-efficients. Once expanded, scattering property of seven individual sub-matrices can be modeled as

$$[T] = f_s\begin{bmatrix}1 & \beta^* & 0\\ \beta & |\beta|^2 & 0\\ 0 & 0 & 0\end{bmatrix} + f_d\begin{bmatrix}|\alpha|^2 & \alpha & 0\\ \alpha^* & 1 & 0\\ 0 & 0 & 0\end{bmatrix} + \frac{f_v}{4}\begin{bmatrix}2 & 0 & 0\\ 0 & 1 & 0\\ 0 & 0 & 1\end{bmatrix} + \frac{f_c}{2}\begin{bmatrix}0 & 0 & 0\\ 0 & 1 & \pm j\\ 0 & \mp j & 1\end{bmatrix} + \frac{f_{od}}{2}\begin{bmatrix}1 & 0 & \pm 1\\ 0 & 0 & 0\\ \pm 1 & 0 & 1\end{bmatrix} + \frac{f_{cd}}{2}\begin{bmatrix}1 & 0 & \pm j\\ 0 & 0 & 0\\ \mp j & 0 & 1\end{bmatrix} + \frac{f_{md}}{2}\begin{bmatrix}0 & 0 & 0\\ 0 & 1 & \pm 1\\ 0 & \pm 1 & 1\end{bmatrix}. \quad (3)$$

As from Figure 1, the first pair of transformation equations, through which the measured coherency matrix is rotated along the radar illumination can be given by

$$[T(\varphi_1)] = [U(\varphi_1)][T][U(\varphi_1)]^\dagger, \quad (4)$$

$$[T(\varphi_2)] = [U(\varphi_2)][T(\varphi_1)][U(\varphi_2)]^\dagger \quad (5)$$

where, $[U(\varphi_1)]$ and $[U(\varphi_2)]$ represents a pair of 3×3 special unitary rotation matrix which possess the property of $[U]^{-1} = [U]^\dagger$ and $det[U] = 1$. Additionally, "†" denotes the Hermitian conjugate of a matrix. They are incorporated to break the coupling of dihedral-volume cross-correlation element, and can be written as

$$[U(\varphi_1)] = \begin{bmatrix}1 & 0 & 0\\ 0 & \cos 2\varphi_1 & \sin 2\varphi_1\\ 0 & -\sin 2\varphi_1 & \cos 2\varphi_1\end{bmatrix}, \quad (6)$$

$$[U(\varphi_2)] = \begin{bmatrix}1 & 0 & 0\\ 0 & \cos 2\varphi_2 & j\sin 2\varphi_2\\ 0 & j\sin 2\varphi_2 & \cos 2\varphi_2\end{bmatrix}. \quad (7)$$

The rotation angles φ_1 and φ_2 can simply be derived by minimizing the cross-polarization component of (4) and (5) respectively. After the accomplishment of double unitary transformation, one can get the rotated elements of the coherency matrix for performing the decomposition [22], [24].

$$\varphi_1 = \frac{1}{4}\tan^{-1}\left\{\frac{2\Re(T_{23})}{T_{22} - T_{33}}\right\}, \quad (8)$$

$$\varphi_2 = \frac{1}{4}\tan^{-1}\left\{\frac{2\Im\{T_{23}(\varphi_1)\}}{T_{22}(\varphi_1) - T_{33}(\varphi_1)}\right\}. \quad (9)$$

Neutralization of surface-volume cross-correlation element can be accomplished through the de-correlation of coupling present in between $\Re/\Im(T_{13})$ element. A set of equations through which (1) is rotated individually with unitary

$$[T] = \begin{bmatrix}T_{11} & T_{12} & T_{13}\\ T_{12}^* & T_{22} & T_{23}\\ T_{13}^* & T_{23}^* & T_{33}\end{bmatrix} = \begin{bmatrix}\frac{1}{2}|S_{HH} + S_{VV}|^2 & \frac{1}{2}(S_{HH} + S_{VV})(S_{HH} - S_{VV})^* & (S_{HH} + S_{VV})S_{HV}^*\\ \frac{1}{2}(S_{HH} - S_{VV})(S_{HH} + S_{VV})^* & \frac{1}{2}|S_{HH} - S_{VV}|^2 & (S_{HH} - S_{VV})S_{HV}^*\\ S_{HV}(S_{HH} + S_{VV})^* & S_{HV}(S_{HH} - S_{VV})^* & 2|S_{HV}|^2\end{bmatrix}. \quad (1)$$

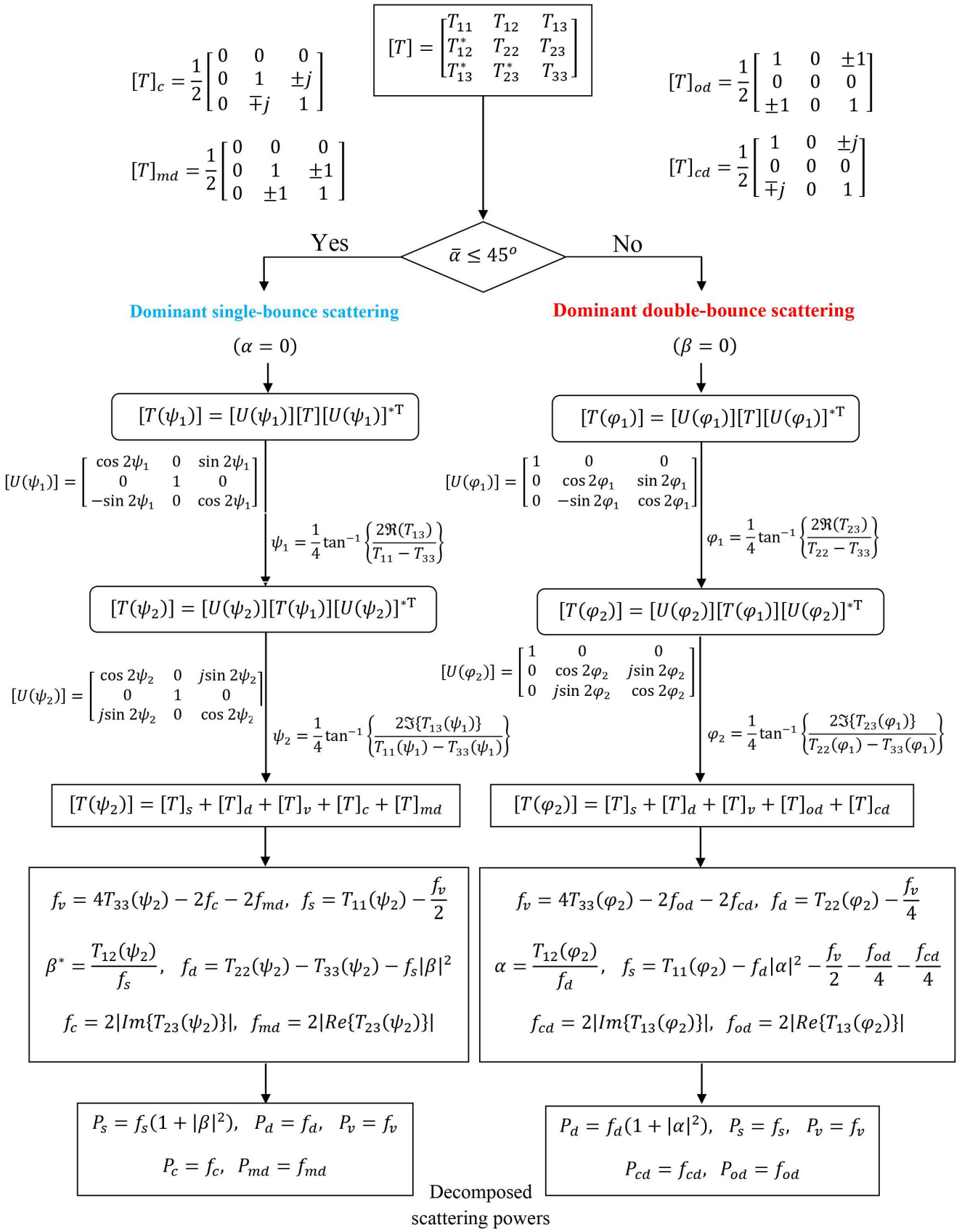

FIGURE 1. Flowchart of the proposed seven-component decomposition (*7SR*) method.

rotations matrices along the line of sight of the radar can be given by

$$[T(\psi_1)] = [U(\psi_1)][T][U(\psi_1)]^{\dagger}, \tag{10}$$

$$[T(\psi_2)] = [U(\psi_2)][T(\psi_1)][U(\psi_2)]^{\dagger} \tag{11}$$

The second pair of incorporated special unitary rotations matrices can be represented as

$$[U(\psi_1)] = \begin{bmatrix} \cos 2\psi_1 & 0 & \sin 2\psi_1 \\ 0 & 1 & 0 \\ -\sin 2\psi_1 & 0 & \cos 2\psi_1 \end{bmatrix}, \tag{12}$$

$$[U(\psi_2)] = \begin{bmatrix} \cos 2\psi_2 & 0 & j\sin 2\psi_2 \\ 0 & 1 & 0 \\ j\sin 2\psi_2 & 0 & \cos 2\psi_2 \end{bmatrix}. \tag{13}$$

The rotation angles ψ_1 and ψ_2 can be calculated by minimizing $T_{33}(\psi_1)$ and $T_{33}(\psi_2)$ element of $[T(\psi_1)]$ and $[T(\psi_2)]$, obtained after the unitary transformation or by determining the null angle for $\Re\{T_{13}(\psi_1)\}$ and $\Im\{T_{13}(\psi_2)\}$, indicated as

$$\psi_1 = \frac{1}{4}\tan^{-1}\left\{\frac{2\Re(T_{13})}{T_{11}-T_{33}}\right\}, \tag{14}$$

$$\psi_2 = \frac{1}{4}\tan^{-1}\left\{\frac{2\Im\{T_{13}(\psi_1)\}}{T_{11}(\psi_1)-T_{33}(\psi_1)}\right\}. \tag{15}$$

Elements of the coherency matrix $[T(\psi_1)]$ and $[T(\psi_2)]$ can now easily be obtained after the accomplishment of the dual unitary transformation [26].

The proper segregation and classification of the terrain depend on the branching condition's potential that is being used. Hence, in the proposed work, to decide the dominant scattering mechanism, branching condition based on the mean alpha ($\overline{\alpha}$) angle has been chosen [37]. Relying upon its elicit, transformation equations (4) and (5) or (10) and (11) can then be implemented to determine the unknowns, followed by the determination of decomposed scattering power.

For a scenario where surface scattering mechanism is supposed to be dominant, by incorporating transformation equation (10) in coordination with the rotation angle ψ_1 (14), the element $\Re(T_{13})$ can be decoupled. Meanwhile, equation (11), along with the rotation angle ψ_2 (15) neutralizes the $\Im(T_{13})$ element. As these eliminations are accounted for the oriented and compounded-dipole scattering hence, one can now only be left with scattering analogous to helix and mixed-dipole accompanying the three basic scattering components. After dual unitary rotations are accomplished, the unknowns can be written as

$$f_v = 4\{T_{33}(\psi_2)\} - 2f_c - 2f_{md},\ \ f_s = T_{11}(\psi_2) - \frac{f_v}{2}$$
$$\beta^* = \frac{\{T_{12}(\psi_2)\}}{f_s},\ \ f_d = T_{22}(\psi_2) - \frac{f_v}{4} - \frac{f_c}{2} - \frac{f_{md}}{2} - f_s|\beta|^2. \tag{16}$$

The modified model corresponding to dominant surface scattering can be given by

$$[T(\psi_2)] = f_s[T]_s + f_d[T]_d + \frac{f_v}{4}[T]_v + \frac{f_c}{2}[T]_c + \frac{f_{md}}{2}[T]_{md}. \tag{17}$$

The scattering power analogous to helix and mixed-dipole scattering are

$$P_c = f_c = 2|\Im\{T_{23}(\psi_2)\}|,\ \ P_{md} = f_{md} = 2|\Re\{T_{23}(\psi_2)\}|. \tag{18}$$

As converse, if the dominant scattering mechanism would be the dihedral, then, *OAC* (4) in coordination with angle φ_1 (8) can be implemented for the de-correlation of $\Re(T_{23})$ element. Furthermore, equation (5), along with angle φ_2 (9) neutralizes the $\Im(T_{23})$ element through helix angle compensation (*HAC*). Hence, mixed-dipole and helix scattering component, which has been accounted through $\Re/\Im(T_{23})$ element is now eliminated. Consequently, oriented and compounded-dipole scattering only remain following the surface, dihedral, and volume scattering component. The unknowns can be determined as

$$f_v = 4\{T_{33}(\varphi_2)\} - 2f_{od} - 2f_{cd},\ \ f_d = T_{22}(\varphi_2) - \frac{f_v}{4}$$
$$\alpha = \frac{\{T_{12}(\varphi_2)\}}{f_d},\ \ f_s = T_{11}(\varphi_2) - f_d|\alpha|^2 - \frac{f_v}{2} - \frac{f_{od}}{2} - \frac{f_{cd}}{2}. \tag{19}$$

The model obtained after the above transformations for the dominant dihedral scattering can now be written as

$$[T(\varphi_2)] = f_s[T]_s + f_d[T]_d + \frac{f_v}{4}[T]_v + \frac{f_{od}}{2}[T]_{od} + \frac{f_{cd}}{2}[T]_{cd}. \tag{20}$$

The scattering power corresponding to the oriented and compounded-dipole scattering are

$$P_{cd} = f_{cd} = 2|\Im\{T_{13}(\varphi_2)\}|,\ \ P_{od} = f_{od} = 2|\Re\{T_{13}(\varphi_2)\}|. \tag{21}$$

The decomposed scattering power associated with the surface, dihedral, and volume scattering mechanism can be given by

$$P_s = f_s\left(1+|\beta|^2\right),\ \ P_d = f_d\left(1+|\alpha|^2\right),\ \ P_v = f_v. \tag{22}$$

The methodology shows that scattering power concerning two sub-scattering mechanisms has been obtained, per pixel for each dominant scattering scenario accompanying the surface, dihedral, and volume. Hence, the strategy completely utilizes nine out of nine coherency matrix elements, giving seven scattering components, per patch during each pair of rotation.

III. EXPERIMENTAL RESULT AND DISCUSSION

Datasets of ALOS PALSAR 2 over the Bay Area and Mumbai are deployed to validate the applicability of the 7*SR* decomposition strategy. In an attempt to observe the specific polarimetric backscattering, four non-identical patches have been selected. They can be represented as vegetation, orthogonal urban settlements, oriented man-made structures, and water surface. Overall, one can conclude that the chosen area of interest represents an entirely natural and

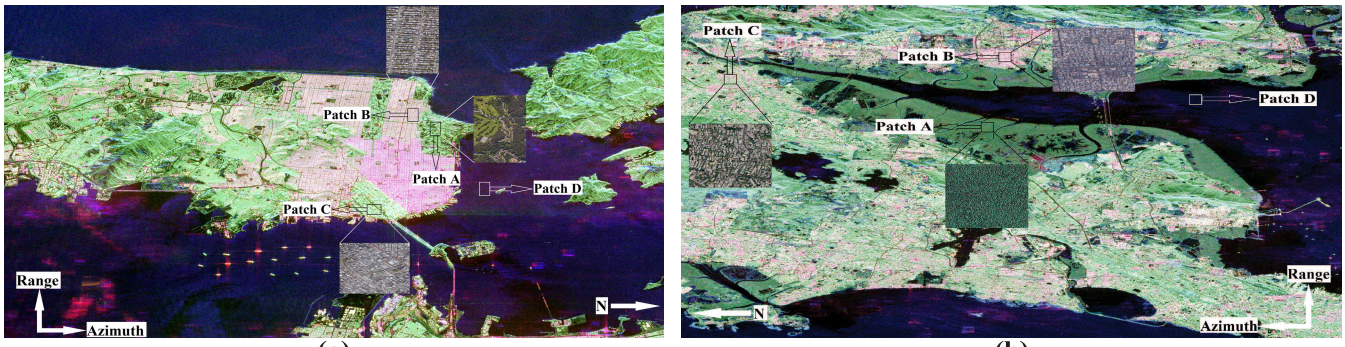

FIGURE 2. Pauli RGB image of (a) Bay Area and (b) Mumbai acquired from ALOS PALSAR-2. Selected Patches belonging to specified terrain has been indicated along with their visual references (Source: Google Earth).

geographical diversity suitable to perform the quantitative analysis. 7*SR* has comparatively been studied against the existing 7*SD* decomposition method through the color-coded decomposed images, taking into consideration the normalized mean scattering power. Additionally, the analysis of negative scattering pixels has also been done. In this investigation, the assignment of colors to indicate backscattering from diverse terrains is as follows: Blue: surface scattering (P_s), Red: double-bounce scattering (P_d), and Green: volume scattering (P_v).

A. ANALYSIS OF DECOMPOSED SCATTERING POWER

The productivity of the 7*SD* and 7*SR* approach and its compatibility to the datasets has been validated and reported in Table 1 and 2 in context to normalized mean scattering powers. While implementing the 7*SD* in both the images for patch A, it is observed that volume scattering power has drastically been reduced even though vegetation is prevalent in this terrain. For the Bay area, P_v is 15.62% while for Mumbai, it becomes 18.35%. This observation can be validated upon analyzing decomposed images of Figures 3 and 4, obtained from 7*SD* methods, where the volume scattering prevalent areas have been wiped off. To a certain extent, 7*SD* justifies the reason for being favorable to the magnification of P_s and P_d as cross-polarization power is being minimized here. Hence, an enhancement in the surface and dihedral scattering power have been observed. In 7*SD*, the P_v can be estimated as

$$P_v = 4T_{33} - 2P_c - 2P_{od} - 2P_{cd} - 2P_{md} \tag{23}$$

With the reference of (23), to determine the power analogous to volume scattering, followed by the solution of the unknowns, contributions of the helix and compounded scattering powers have been subtracted from the cross-polarization component. Aforementioned strategy triggered the case of underestimation in P_v as it is determined through T_{33} from which the power associated with four sub-scattering mechanisms has been excluded. With such uncertainty, it might be concluded that the existing model is not compatible with the vegetated terrain. However, the specified area's forested characteristics have been retained when

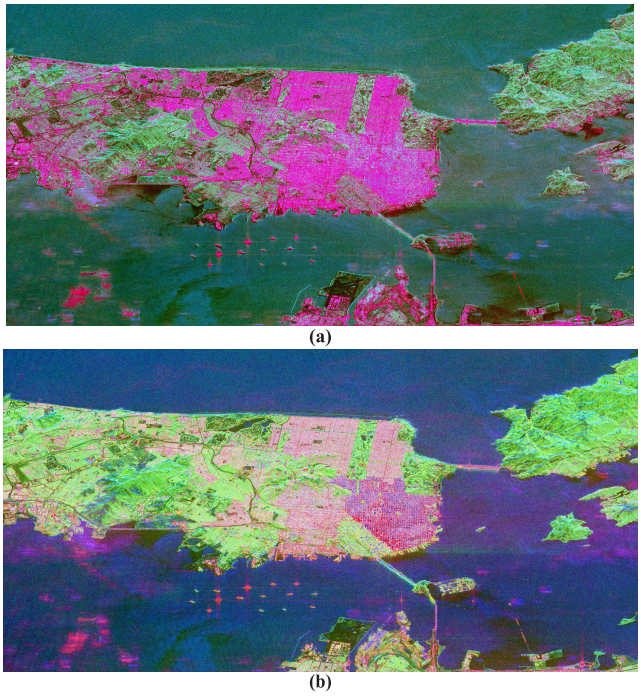

FIGURE 3. Decomposed color coded images of ALOS PALSAR-2, Bay Area, CA. (a) *7SD* (b) *7SR*.

the analysis is carried out through the 7*SR* approach. The volume scattering power remains dominant and saturated to a value of 45.21% and 42.80% for both the images, which is justified and much higher than the parallel 7*SD* method.

Further moving on the statistics of urban patch B, the dihedral scattering is predominantly observed as the area is situated orthogonal to the radar illumination. Hence, one can observe a satisfactory enhancement in the percentage of even-bounce scattering power as the two structures are perpendicular to each other and eventually generated the condition of scattering from the dihedral. For these two images, the percentage of pixels classified as dihedral using the proposed 7*SR* method are 52.09% and 65.06% respectively, which is 3.52% and 1.36% higher than that suggested by 7*SD*.

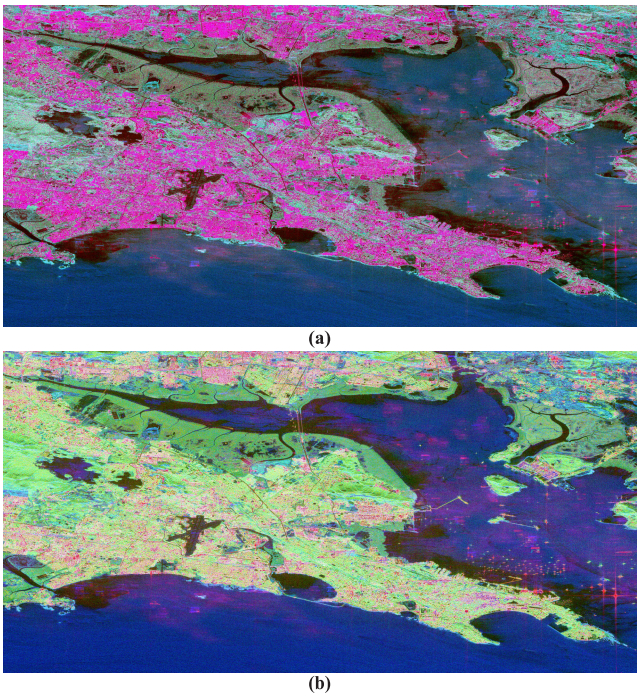

FIGURE 4. Decomposed color coded images of ALOS PALSAR-2, Mumbai. (a) *7SD* (b) *7SR*.

TABLE 1. Normalized mean scattering powers (in %) over the specified patches of bay area.

Methods	Patch A (Vegetation)						
	P_s	P_d	P_v	P_c	P_{md}	P_{od}	P_{cd}
7*SD*	34.69	22.88	15.62	5.50	5.89	7.79	7.65
Proposed 7*SR*	**20.41**	**21.41**	**45.21**	**1.83**	**1.85**	**4.70**	**4.58**

Methods	Patch B (Urban)						
	P_s	P_d	P_v	P_c	P_{md}	P_{od}	P_{cd}
7*SD*	32.87	48.57	3.64	3.70	8.12	2.00	1.10
Proposed 7*SR*	**30.81**	**52.09**	**7.74**	**0.81**	**1.25**	**3.65**	**3.64**

Methods	Patch C (Complex Urban)						
	P_s	P_d	P_v	P_c	P_{md}	P_{od}	P_{cd}
7*SD*	25.52	23.70	12.67	6.59	10.97	10.70	9.46
Proposed 7*SR*	**7.03**	**21.26**	**52.82**	**1.10**	**1.58**	**8.47**	**7.75**

Methods	Patch D (Sea)						
	P_s	P_d	P_v	P_c	P_{md}	P_{od}	P_{cd}
7*SD*	66.41	20.76	11.41	0.37	0.41	0.33	0.32
Proposed 7*SR*	**70.39**	**19.88**	**5.50**	**2.00**	**2.22**	**0.0067**	**0.0074**

Referring to methodology (ref. Figure 1), due to the incorporation of unitary rotations, elements $\Re(T_{23})$ and $\Im(T_{23})$ are eliminated. As a consequence, terms $\Re(T_{23})\, sin4\varphi_1$ and $\Im\{T_{23}(\varphi_1)\}\, sin4\varphi_2$ are subtracted from the cross-polarization component and concurrently added to T_{22}, which further

TABLE 2. Normalized mean scattering powers (in %) over the specified patches of Mumbai.

Methods	Patch A (Vegetation)						
	P_s	P_d	P_v	P_c	P_{md}	P_{od}	P_{cd}
7*SD*	39.76	21.58	18.35	4.32	4.29	5.76	5.95
Proposed 7*SR*	**30.42**	**17.48**	**42.80**	**2.44**	**2.36**	**2.21**	**2.28**

Methods	Patch B (Urban)						
	P_s	P_d	P_v	P_c	P_{md}	P_{od}	P_{cd}
7*SD*	23.18	63.70	1.46	2.70	6.39	1.91	0.66
Proposed 7*SR*	**26.53**	**65.06**	**1.92**	**0.31**	**0.64**	**2.83**	**2.71**

Methods	Patch C (Complex Urban)						
	P_s	P_d	P_v	P_c	P_{md}	P_{od}	P_{cd}
7*SD*	31.52	32.70	9.77	5.57	8.95	6.32	5.17
Proposed 7*SR*	**21.40**	**29.40**	**36.71**	**1.09**	**1.35**	**5.11**	**4.94**

Methods	Patch D (Sea)						
	P_s	P_d	P_v	P_c	P_{md}	P_{od}	P_{cd}
7*SD*	81.45	8.55	9.36	0.14	0.13	0.19	0.18
Proposed 7*SR*	**84.35**	**7.68**	**5.39**	**1.30**	**1.27**	**0.01**	**0.01**

strengthens the dihedral scattering mechanism. Simultaneously, urban areas with minimal T_{33} can be segregated and classified more effectively.

However, the decomposed RGB images of Figures 3 and 4 obtained through the 7*SD* method is not justifying the outcomes of the quantitative analysis of Table 1 and 2. Against 7*SR*, these areas appear to be more segregated as magenta appearance is widespread. Hence, at first glance, the result might seem to be contradictory from solely the classification accuracy viewpoint. Nevertheless, in an actual scenario, it all depends on how the algorithm is treating with the contributions from P_v. In 7*SD*, most of the power associated with the volume scattering is negative. Consequently, their contribution has been made zero incorporating power restriction constraints. As color is concerned, in an RGB image of the decomposed terrain, green color is designated for the volume scattering power. If the contribution of green is being vanished form the particular pixel, then one can only be left with blue and red color representing odd and even bounce power, which gives magenta texture to the urban terrain (ref. Figure 5). However, the 7*SR* approach has been carried out without considering any power restriction constraints. So, the urban area appears light red in the decomposed images. Hence, apart from the dominant dihedral scattering, contributions from different scattering mechanism have been retained for each pixel.

Dihedral backscattering from the orthogonal structures are not similar to that of the oriented man-made settlements. For the latter, the main scattering center is situated at an oblique direction with respect to the radar line of sight.

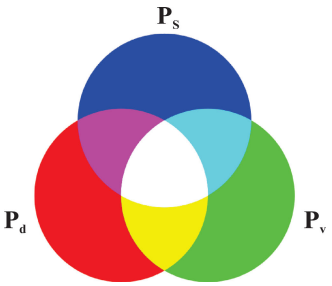

FIGURE 5. The color wheel.

Classification of such complex settlements is considered one of the significant challenges in order to validate the productivity of any decomposition algorithm. Obeying it, patch C has been selected which is supposed to show the even-bounce but actually gets dominated by the multiple scatterings.

Performing the analysis for patch C, 7*SD* gives P_d equivalent to 23.70% and 32.70% for both the datasets. However, dihedral contribution for Bay area seems to be low compared to the enhancement in its odd-bounce counterpart, which has become dominant here. Additionally, the collective contributions from the four sub-scattering components are 37.72% and 26.01%. The outcomes are much higher and justify the presence of cross-polarization power in these complex man-made settlements. Furthermore, adding the contributions of helix and compounded scattering power to the concerned scattering mechanism for the Bay area, i.e., P_{od}, P_{cd} to P_s and P_c, P_{md} to P_d, shows the dominance of P_s over P_d by 4.42%. So, despite using the complex polarimetry information through the additional four scattering components, the performance of 7*SD* remains sub-optimal.

In parallel, the proposed 7*SR* approach for Patch C gives P_s, P_d and P_v equivalent to 7.03%, 21.26% and 52.82% for the Bay Area image. While for Mumbai, it comes out to be 21.40%, 29.40%, and 36.71%. Hence, a degradation of 2.44% and 3.30% in the amount of dihedral scattering power has been observed compared to that obtained for 7*SD*. Individual pixels show contributions from the five scattering components, as a cross-correlation component gets removed after each pair of rotation. Simultaneously, their scattering information can't be considered. Hence, a slight reduction in the percentage of P_d is observed, which is fair enough as it efficiently reduces P_s to 18.49% and 10.12% for both the images. Following the complex nature of the environment, P_v has been magnified. Nevertheless, considering challenges, the 7*SR* decomposition strategy has maintained the accuracy by making the pixels non-negative. For the water patch D, 7*SR* method classifies 70.39% and 84.35% pixels in favor of P_s for both the Bay area and Mumbai images. Meanwhile, for 7*SD*, the percentage of pixels for which P_s dominates is 66.41% and 81.45%, which is 3.98% and 2.9% lower than the proposed method.

B. ANALYSIS OF NEGATIVE SCATTERING PIXELS

Analysis related to negative scattering power pixels for both the images has been shown in Table 3 and 4.

TABLE 3. Amount of negative scattering pixels (in %) over the entire region of interest of bay area image.

Methods	7*SD*	7*SR*
Negative power pixels	72.46	**17.16**

TABLE 4. Amount of negative scattering pixels (in %) over the entire region of interest of Mumbai image.

Methods	7*SD*	7*SR*
Negative power pixels	71.62	**19.37**

It is noted that for 7*SD*, more than 70% of the pixels estimated negative power for one of the components, and for most of the cases, the pixels under question are associated with the volume scattering power. Here, most of the cross-polarized power has been assigned for the magnification of P_s and P_d, which severely underestimates the volume scattering contribution. For the Bay Area image, the number of pixels where the power constraints have been added to forcefully make them non-negative is 72.46%. While, for the Mumbai image, it is 71.62%. Additionally, with the increase in components, the main emphasis has been on enhancing the classification accuracy by utilizing the complete polarimetry information. Hence, in 7*SD*, deorientation processing has been removed so as to preserve the polarimetric information. An enhancement in classification accuracy is surely observed as targets can better be characterized by the inclusion of compounded scattering power due to the mixed dipoles. However, the approach makes the algorithm more complex as the number of unknowns increases. So, there is a need for an adaptive technique that can detect the cross-polarization power generated from the single, double-bounce, and volume scattering components accurately.

Through the 7*SR* framework, the uncertainty of volume scattering power can now be intercepted. For each prevailing scattering scenario, one can have a different set of equations for P_v, determined by subtracting the contributions from only two sub-scattering components. For the case where surface scattering mechanism is dominant, the volume scattering power can be determined, subtracting the contributions of the helix and mixed-dipole scattering from the rotated cross-polarization component as

$$P_v = 4\{T_{33}(\psi_2)\} - 2P_c - 2P_{md}. \tag{24}$$

While, if scattering form dihedral is prevalent, contributions from the oriented and compounded-dipole scattering have been subtracted from the minimized T_{33} component. Volume scattering power can then be calculated as

$$P_v = 4\{T_{33}(\varphi_2)\} - 2P_{od} - 2P_{cd}. \tag{25}$$

A drastic reduction in the percentage of negative scattering pixels has been observed when the datasets have been

processed through the proposed 7*SR* algorithm. For the Bay Area image, the percentage of such pixels is reduced to 17.16% which is 55.3% improved in context to 7*SD*. Meanwhile, Mumbai image shows only 19.37% of pixels as negative, which is 52.25% better in contrast to 71.62% using 7*SD*. Through the proposed strategy, even after incorporating the unitary rotations, one can get the contributions from the sub-scattering mechanisms. Hence, apart from reducing the overestimation problem, one can also mitigate the underestimation related to the volume scattering power simultaneously, maintaining its compatibility with the terrain.

IV. CONCLUSION

New scattering models and unitary matrix rotations theory have rigorously been studied in context to completely utilize the fully polarimetric coherency matrix's information. Based on that, an improved seven component scattering power decomposition technique has been proposed exploiting the best attributes of both the strategies. By excluding the power restriction constraints, the framework has reduced the algorithmic complexity of the decomposition technique. Hence, the robustness in maintaining the distribution of power among the seven scattering components has more efficiently been explained by the proposed approach against the 7*SD*. Moreover, ambiguities related to the volume scattering power have been tackled by determining it separately for each dominant scattering scenario. Hence, the occurrence of negative scattering pixels has been greatly suppressed.

ACKNOWLEDGMENT

The authors would like to thank JAXA for providing the ALOS PALSAR-2 datasets.

REFERENCES

[1] A. Freeman and S. L. Durden, "A three-component scattering model for polarimetric SAR data," *IEEE Trans. Geosci. Remote Sens.*, vol. 36, no. 3, pp. 963–973, May 1998.

[2] Y. Yamaguchi, T. Moriyama, M. Ishido, and H. Yamada, "Four-component scattering model for polarimetric SAR image decomposition," *IEEE Trans. Geosci. Remote Sens.*, vol. 43, no. 8, pp. 1699–1706, Aug. 2005.

[3] W. An, Y. Cui, and J. Yang, "Three-component model-based decomposition for polarimetric SAR data," *IEEE Trans. Geosci. Remote Sens.*, vol. 48, no. 6, pp. 2732–2739, Jun. 2010.

[4] A. Freeman, "Fitting a two-component scattering model to polarimetric SAR data from forests," *IEEE Trans. Geosci. Remote Sens.*, vol. 45, no. 8, pp. 2583–2592, Aug. 2007.

[5] M. Arii, J. J. van Zyl, and Y. Kim, "A general characterization for polarimetric scattering from vegetation canopies," *IEEE Trans. Geosci. Remote Sens.*, vol. 48, no. 9, pp. 3349–3357, Sep. 2010.

[6] M. Arii, J. J. van Zyl, and Y. Kim, "Adaptive model-based decomposition of polarimetric SAR covariance matrices," *IEEE Trans. Geosci. Remote Sens.*, vol. 49, no. 3, pp. 1104–1113, Mar. 2011.

[7] O. Antropov, Y. Rauste, and T. Hame, "Volume scattering modeling in PolSAR decompositions: Study of ALOS PALSAR data over boreal forest," *IEEE Trans. Geosci. Remote Sens.*, vol. 49, no. 10, pp. 3838–3848, Oct. 2011.

[8] B. Chen, L. Jiao, and S. Zhang, "An improved three-component model-based decomposition for polarimetric SAR data," in *Proc. Int. Conf. Audio, Lang. Image Process.*, Jul. 2014, pp. 419–422.

[9] Z. Wang, Q. Zeng, and J. Jiao, "A new volume scattering model for three-component decomposition of polarimetric SAR data," in *Proc. IEEE Int. Geosci. Remote Sens. Symp. IGARSS*, Jul. 2018, pp. 4575–4578.

[10] A. Sato, Y. Yamaguchi, G. Singh, and S.-E. Park, "Four-component scattering power decomposition with extended volume scattering model," *IEEE Geosci. Remote Sens. Lett.*, vol. 9, no. 2, pp. 166–170, Mar. 2012.

[11] J.-S. Lee, T. L. Ainsworth, and Y. Wang, "Generalized polarimetric model-based decompositions using incoherent scattering models," *IEEE Trans. Geosci. Remote Sens.*, vol. 52, no. 5, pp. 2474–2491, May 2014.

[12] S.-H. Hong and S. Wdowinski, "Double-bounce component in cross-polarimetric SAR from a new scattering target decomposition," *IEEE Trans. Geosci. Remote Sens.*, vol. 52, no. 6, pp. 3039–3051, Jun. 2014.

[13] D. Xiang, Y. Ban, and Y. Su, "Model-based decomposition with cross scattering for polarimetric SAR urban areas," *IEEE Geosci. Remote Sens. Lett.*, vol. 12, no. 12, pp. 2496–2500, Dec. 2015.

[14] D. Xiang, Y. Ban, and Y. Su, "The cross-scattering component of polarimetric SAR in urban areas and its application to model-based scattering decomposition," *Int. J. Remote Sens.*, vol. 37, no. 16, pp. 3729–3752, Jul. 2016.

[15] S. Quan, B. Xiong, D. Xiang, C. Hu, and G. Kuang, "Scattering characterization of obliquely oriented buildings from PolSAR data using eigenvalue-related model," *Remote Sens.*, vol. 11, no. 5, p. 581, Mar. 2019.

[16] H. Maurya, R. K. Panigrahi, and A. K. Mishra, "Extended four-component decomposition by using modified cross-scattering matrix," *IET Radar, Sonar Navigat.*, vol. 11, no. 8, pp. 1196–1202, Jun. 2017.

[17] G. Singh and Y. Yamaguchi, "Model-based six-component scattering matrix power decomposition," *IEEE Trans. Geosci. Remote Sens.*, vol. 56, no. 10, pp. 5687–5704, Oct. 2018.

[18] G. Singh, R. Malik, S. Mohanty, V. S. Rathore, K. Yamada, M. Umemura, and Y. Yamaguchi, "Seven-component scattering power decomposition of PolSAR coherency matrix," *IEEE Trans. Geosci. Remote Sens.*, vol. 57, no. 11, pp. 8371–8382, Nov. 2019.

[19] J. R. Huynen, "Phenomenological theory of radar targets," Ph.D. dissertation, Dept. Electr. Eng., Math. Comput. Sci., Technical Univ., Delft, The Netherlands, 1970.

[20] J. R. Huynen, "Phenomenological theory of radar targets," in *Electromagnetic Scattering*, P. L. E. Uslenghi, Ed. New York, NY, USA: Academic, 1978, ch. 16, pp. 653–712.

[21] F. Xu and Y.-Q. Jin, "Deorientation theory of polarimetric scattering targets and application to terrain surface classification," *IEEE Trans. Geosci. Remote Sens.*, vol. 43, no. 10, pp. 2351–2364, Oct. 2005.

[22] Y. Yamaguchi, A. Sato, W.-M. Boerner, R. Sato, and H. Yamada, "Four-component scattering power decomposition with rotation of coherency matrix," *IEEE Trans. Geosci. Remote Sens.*, vol. 49, no. 6, pp. 2251–2258, Jun. 2011.

[23] J.-S. Lee and T. L. Ainsworth, "The effect of orientation angle compensation on coherency matrix and polarimetric target decompositions," *IEEE Trans. Geosci. Remote Sens.*, vol. 49, no. 1, pp. 53–64, Jan. 2011.

[24] G. Singh, Y. Yamaguchi, and S.-E. Park, "General four-component scattering power decomposition with unitary transformation of coherency matrix," *IEEE Trans. Geosci. Remote Sens.*, vol. 51, no. 5, pp. 3014–3022, May 2013.

[25] A. Bhattacharya, G. Singh, S. Manickam, and Y. Yamaguchi, "An adaptive general four-component scattering power decomposition with unitary transformation of coherency matrix (AG4U)," *IEEE Geosci. Remote Sens. Lett.*, vol. 12, no. 10, pp. 2110–2114, Oct. 2015.

[26] H. Maurya and R. K. Panigrahi, "PolSAR coherency matrix optimization through selective unitary rotations for model-based decomposition scheme," *IEEE Geosci. Remote Sens. Lett.*, vol. 16, no. 4, pp. 658–662, Apr. 2019.

[27] S.-W. Chen, X.-S. Wang, S.-P. Xiao, and M. Sato, "General polarimetric model-based decomposition for coherency matrix," *IEEE Trans. Geosci. Remote Sens.*, vol. 52, no. 3, pp. 1843–1855, Mar. 2014.

[28] Y. Yajima, Y. Yamaguchi, R. Sato, H. Yamada, and W.-M. Boerner, "PolSAR image analysis of wetlands using a modified four-component scattering power decomposition," *IEEE Trans. Geosci. Remote Sens.*, vol. 46, no. 6, pp. 1667–1673, Jun. 2008.

[29] S. R. Cloude, *Polarisation: Applications in Remote Sensing*. London, U.K.: Oxford Univ. Press, 2010.

[30] J. J. van Zyl, M. Arii, and Y. Kim, "Model-based decomposition of polarimetric SAR covariance matrices constrained for nonnegative eigenvalues," *IEEE Trans. Geosci. Remote Sens.*, vol. 49, no. 9, pp. 3452–3459, Sep. 2011.

[31] Y. Cui, Y. Yamaguchi, J. Yang, H. Kobayashi, S.-E. Park, and G. Singh, "On complete model-based decomposition of polarimetric SAR coherency matrix data," *IEEE Trans. Geosci. Remote Sens.*, vol. 52, no. 4, pp. 1991–2001, Apr. 2014.

[32] G. Singh, Y. Yamaguchi, S.-E. Park, Y. Cui, and H. Kobayashi, "Hybrid Freeman/eigenvalue decomposition method with extended volume scattering model," *IEEE Geosci. Remote Sens. Lett.*, vol. 10, no. 1, pp. 81–85, Jan. 2013.
[33] H. Maurya and R. K. Panigrahi, "Non-negative scattering power decomposition for PolSAR data interpretation," *IET Radar, Sonar Navigat.*, vol. 12, no. 6, pp. 593–602, Jun. 2018.
[34] W. An and M. Lin, "A reflection symmetry approximation of multilook polarimetric SAR data and its application to Freeman–Durden decomposition," *IEEE Trans. Geosci. Remote Sens.*, vol. 57, no. 6, pp. 3649–3660, Jun. 2019.
[35] H. Maurya, A. Kumar, A. K. Mishra, and R. K. Panigrahi, "Improved four-component based polarimetric synthetic aperture radar image decomposition," *IET Radar, Sonar Navigat.*, vol. 14, no. 4, pp. 619–627, Apr. 2020.
[36] J. S. Lee and E. Pottier, *Polarimetric Radar Imaging: From Basics to Applications*. New York, NY, USA: Taylor & Francis, Feb. 2009.
[37] H. Maurya and R. K. Panigrahi, "Investigation of branching conditions in model-based decomposition methods," *IEEE Geosci. Remote Sens. Lett.*, vol. 15, no. 8, pp. 1224–1228, Aug. 2018.

AMIT KUMAR (Student Member, IEEE) received the B.E. degree in electronics and communication engineering from the University of Rajasthan, Jaipur, in 2009, and the M.Tech. degree in RF and microwaves from IIT Kharagpur, in 2016. He is currently pursuing the Ph.D. degree in RF and microwaves with the Department of Electronics and Communication Engineering, IIT Roorkee. He was with the Department of Electronics and Communication Engineering, National Institute of Technology at Jamshedpur, as the Teaching Faculty of engineering, until 2018, when he joined IIT Roorkee as a Senior Research Fellow for the NISAR (NASA-ISRO SAR) Project. His primary research interests include high-power microwaves, microwave imaging, polarimetric SAR, and ECM/ECCM techniques.

HIMANSHU MAURYA received the B.E. degree from the Thakral College of Technology, Bhopal, in 2011, the M.Tech. degree from the National Institute of Technology at Patna, in 2013, and the Ph.D. degree from IIT Roorkee, in 2019. From 2019 to 2020, he was a Postdoctoral Researcher Fellow with the University of Cape Town, South Africa. He has worked as the Research Scientist of the North Eastern Space Applications Centre, Meghalaya, from August 2020 to November 2020. He is currently an Assistant Professor with the Indian Institute of Information Technology at Allahabad. His research interests include polarimetric SAR, eigenvector-based and model-based scattering mechanisms decomposition, urban extraction, biomass estimation, and remote sensing of atmosphere.

ARUNDHATI RAY MISRA received the B.E. degree in electronics and communication engineering, in 1984, the M.E. degree in computer science and engineering from Jadavpur University, Calcutta, India, in 1986, and the Ph.D. degree in computer science and engineering from Nirma University, in 2017. Since 1986, she has been with SAC, ISRO, and involved in the development of SAR signal processing algorithm. She designed and developed the processor for JPL's SEASAT (*L*-band) SAR data. She designed and developed the ERS-1 SAR processor which was operationalized at NRSA, Hyderabad, in 1991. She contributed extensively to the design and development of a parallel processor-based SAR processing algorithm, developed on PARAM machine of CDAC, India, which was the first indigenous Super Computer of India using multiple Transputers as the backend processors. She was designated as the Project Manager (DP) of ISRO's Multi-frequency Scanning Microwave Radiometer (MSMR). She was also designated as the Deputy Project Director of data products for the Joint ISRO-CNES Project, "Meghatropiques." She was involved in spaceborne millimeter wave sounder simulation and configuration studies of spaceborne millimeter wave sounder for Temperature and Humidity Sounding (TSU and HSU) of ISRO. She was deputed as the Guest Scientist to DLR, Germany, where she designed and developed the DInSAR processor for ESAR, sensor. She is also involved in the hyperspectral technique development activities in SAC. Her research interests include SAR, radiometer, scatterometer, mm-sounder, interferometric SAR, polarimetric SAR, wavelet-based studies, and hyperspectral techniques development. She is also the Group Director of the Advanced Microwave and Hyperspectral Technique Development Group, in SAC, ISRO, Ahmedabad.

RAJIB KUMAR PANIGRAHI (Senior Member, IEEE) received the B.E. degree in electronics and communication engineering from Bangalore University (Now VTU), the M.Tech. degree in electronics with specialization in microwave engineering from the Cochin University of Science and Technology, and the Ph.D. degree from IIT Guwahati, in 2011. Since 2012, he has been with the Department of Electronics and Communication Engineering, IIT Roorkee, where he is currently an Associate Professor. His research interests include radar-based remote sensing, SAR image denoising, segmentation and classification of SAR images, radar interferometry, and radar polarimetry.